Supporting Information for

p-d hybridized Single-atom Catalysts based on Covalent-bond-linked Fullerene Monolayer Network for CO_2 Reduction

Manfu Li[1], Zhilin Liu[1], Guang Yang[1], Xiaoyan Ren,[1,*] and Shunfang Li[1,2,†]

[1]Key Laboratory of Material Physics, Ministry of Education, School of Physics, Zhengzhou University, Zhengzhou 450001, China

[2]Institute of Quantum Materials and Physics, Henan Academy of Sciences, Zhengzhou 450046, China

E-mails: renxyan@zzu.edu.cn; sflizzu@zzu.edu.cn

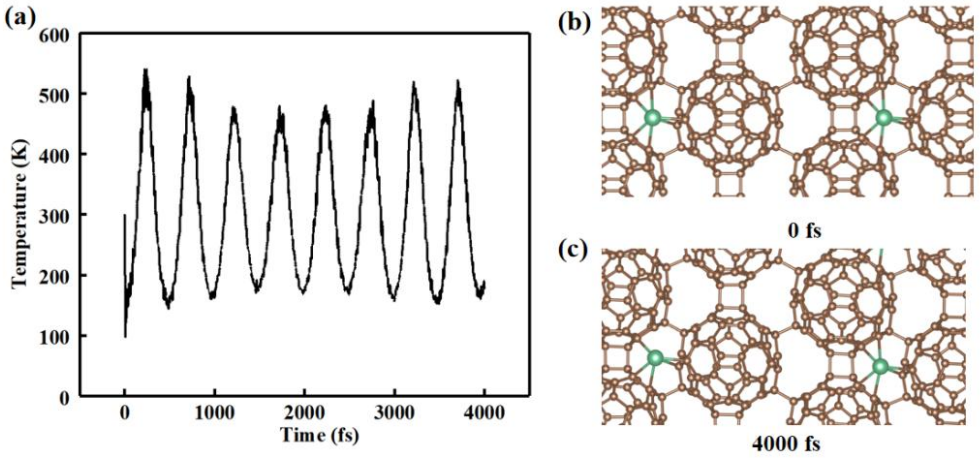

Fig. S1 Ab initio molecular dynamics (AIMD) simulations of the Nb_1@qHP-C_{60} system at 300 K over 4 ps.

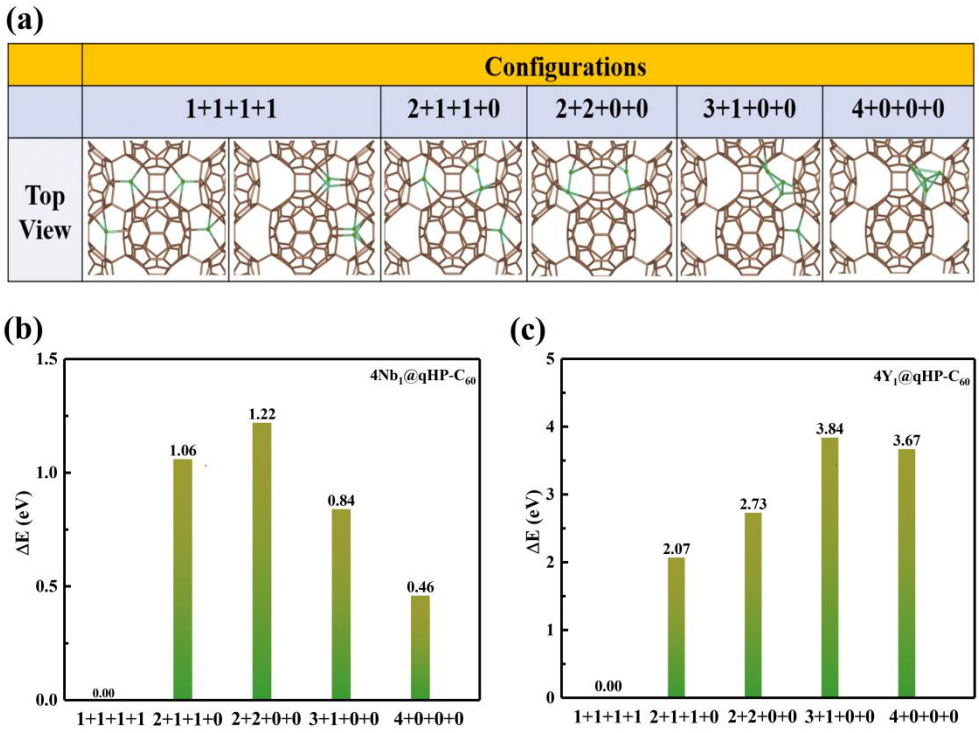

Fig. S2 (a) Optimized configurations of four transition metal atoms on the 2D qHP-C_{60} surface; Relative energies of various configurations formed by the deposition of four Nb (b) and four Y (c) atoms on the 2D qHP-C_{60} surface.

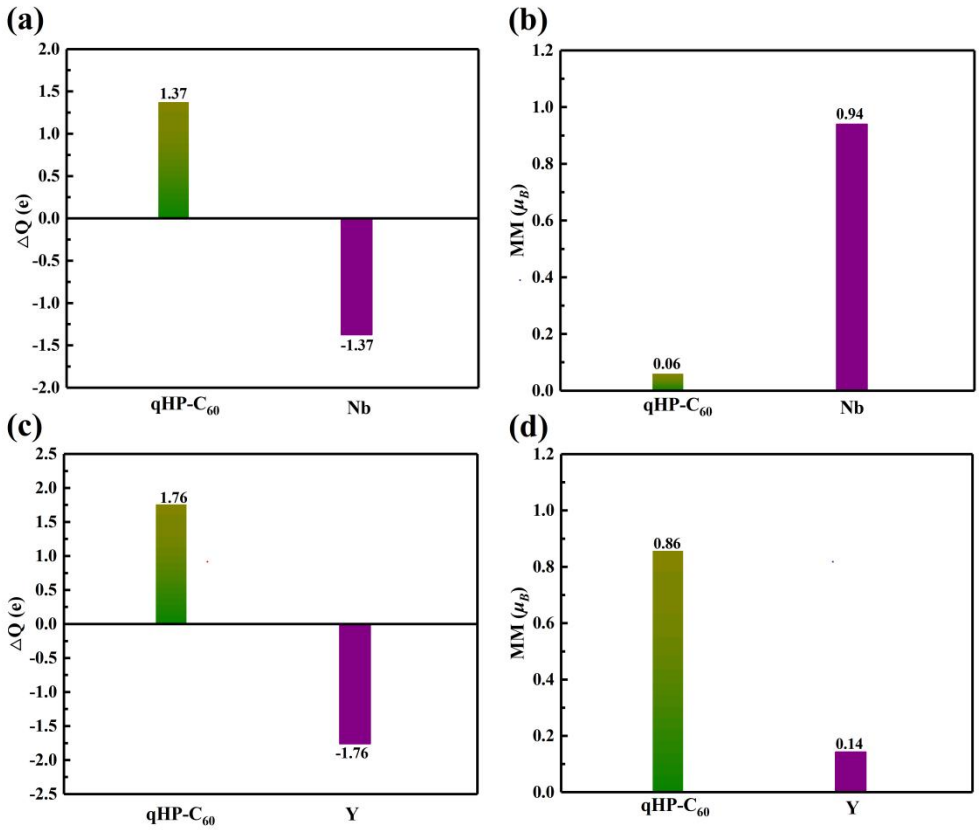

Fig. S3 Charge transfer and magnetic moment variations induced by the deposition of a single Nb or Y atom onto the 2D qHP-C_{60} surface: (a) charge transfer and (b) magnetic moment of Nb system; While (c) and (d) represent those of Y.

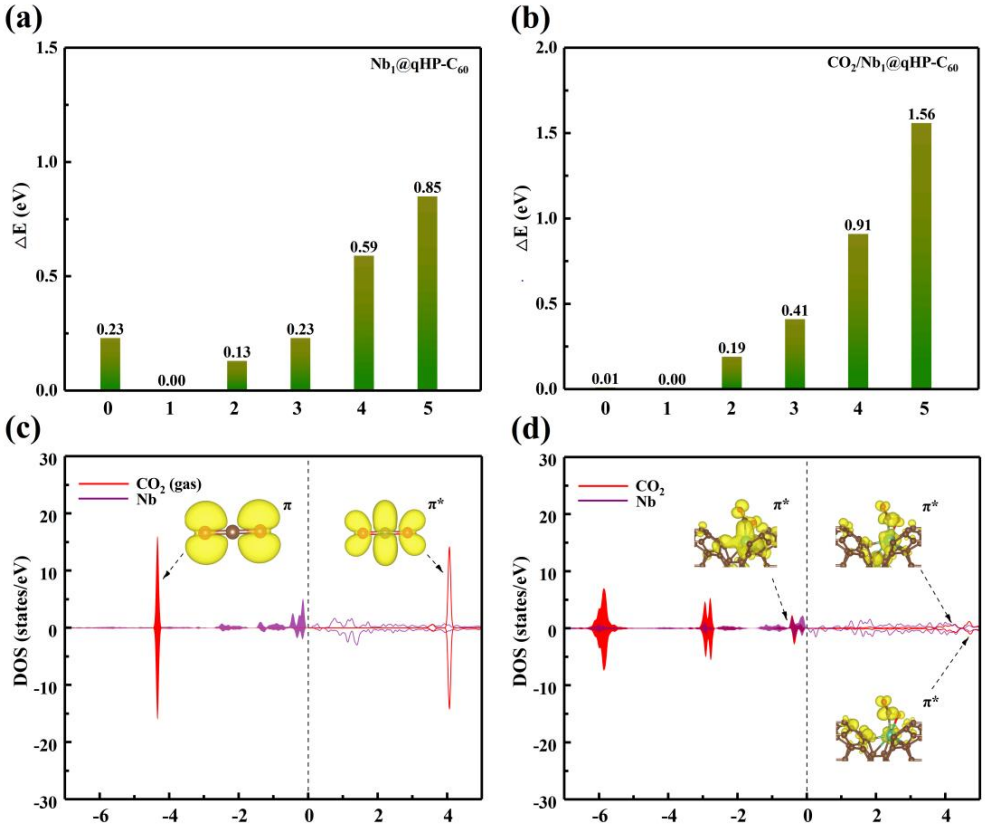

Fig. S4 (a) Relative energies of the Nb_1@qHP-C_{60} system and (b) the CO_2/Nb_1@qHP-C_{60} system under varying magnetic moments; Orbital charge density distributions before (c) and after (d) CO_2 adsorption.

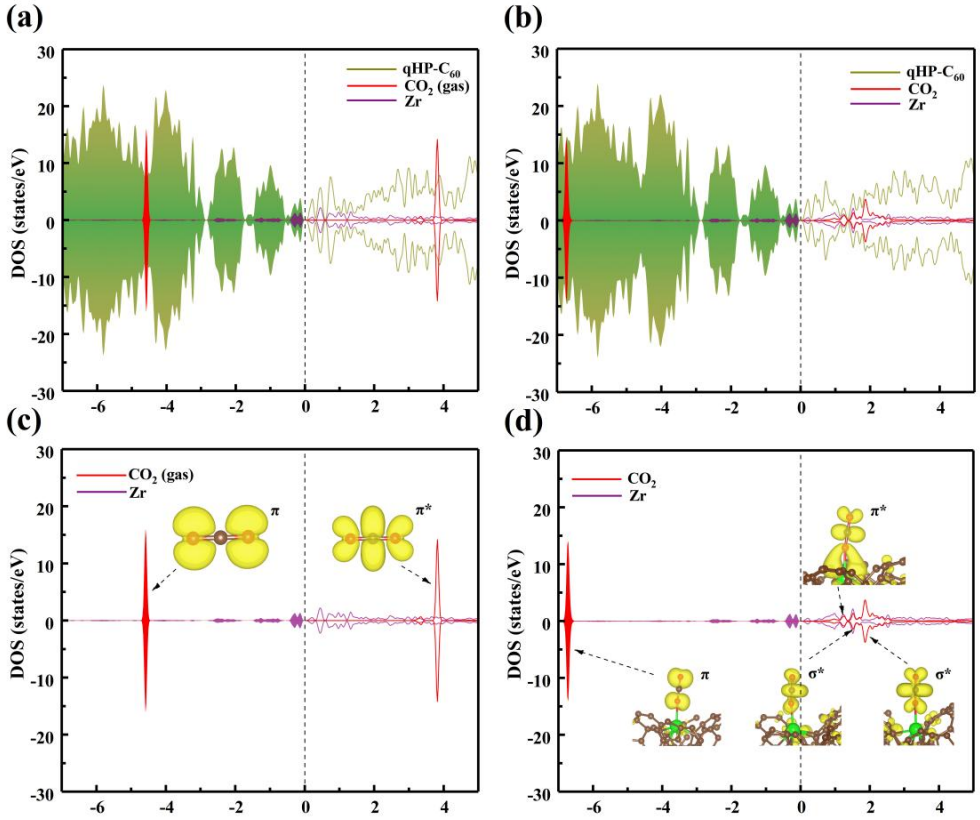

Fig. S5 In the Zr_1@qHP-C_{60} system, the electronic density of states of the CO_2 molecule before (a) and after (b) adsorption, as well as the orbital charge density distributions before (c) and after (d) adsorption.

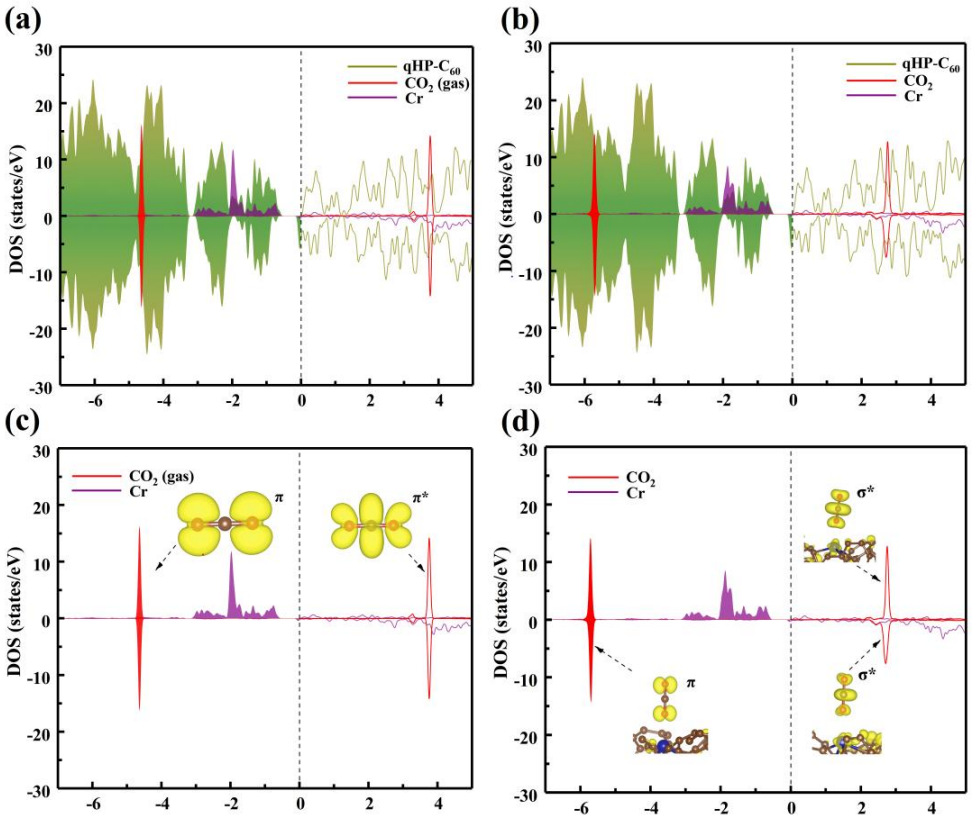

Fig. S6 In the Cr_1@qHP-C_{60} system, the electronic density of states of the CO_2 molecule before (a) and after (b) adsorption, as well as the orbital charge density distributions before (c) and after (d) adsorption.

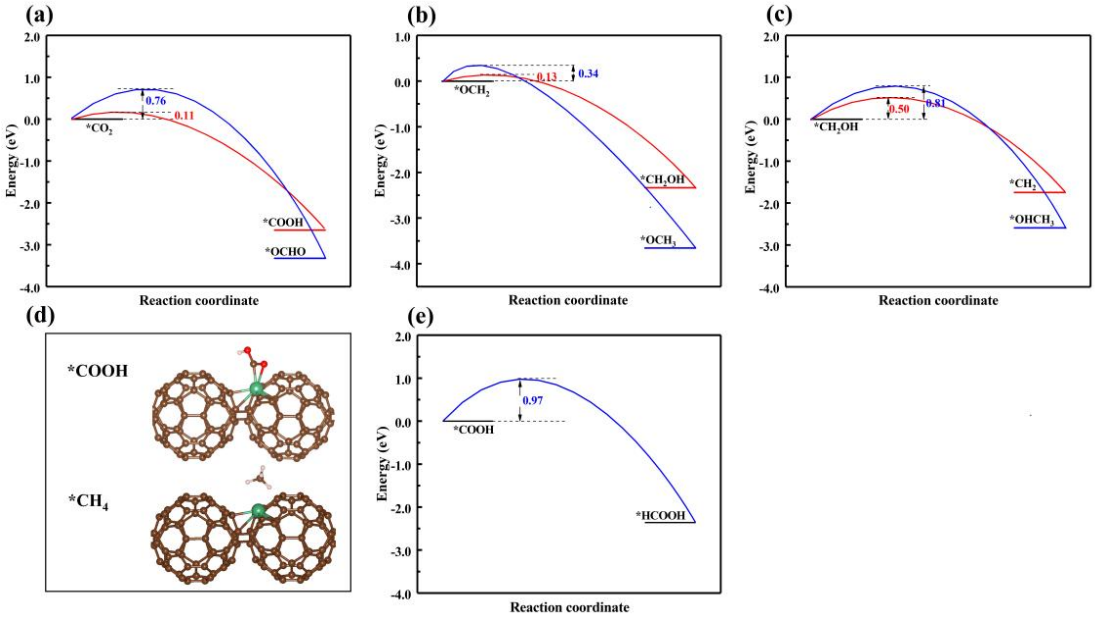

Fig. S7 The protonation barriers of (a) *CO_2, (b) *OCH_2, (c) *CH_2OH, (e) *COOH; (d) The configurations of *COOH and *CH_4.

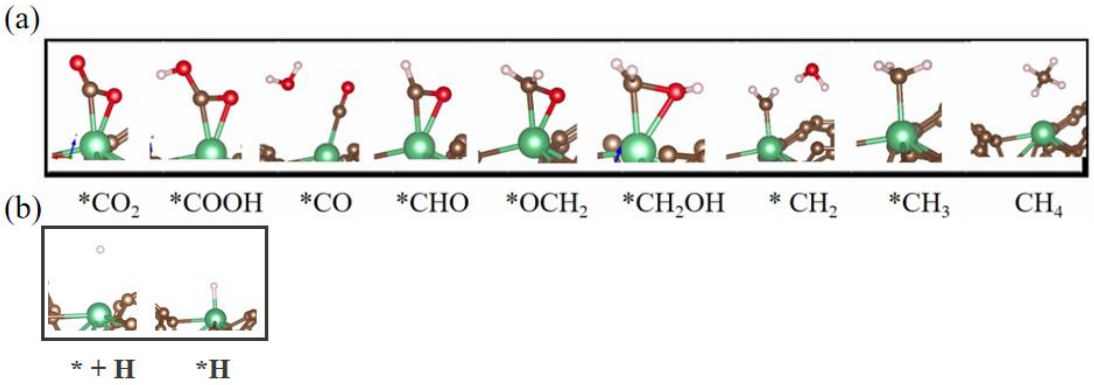

Fig. S8: Optimized geometries of all critical intermediates along the most favorable reaction route for (a) CO_2RR and (b) HER on Nb_1@qHP-C_{60}.

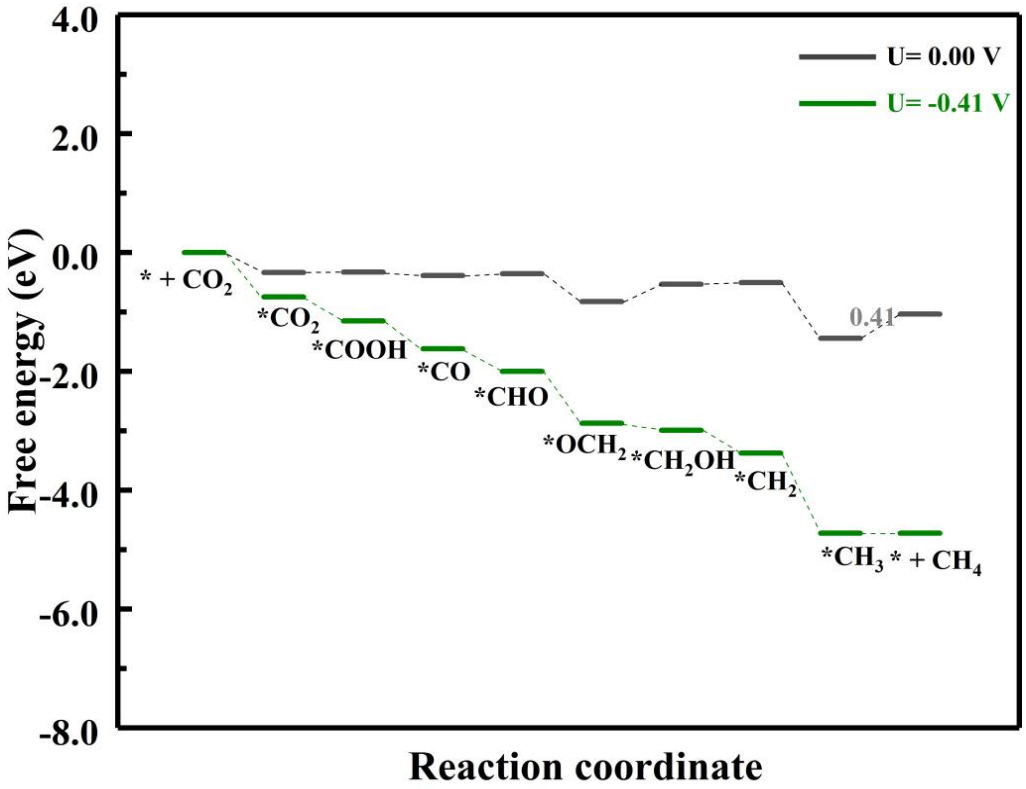

Fig. S9 The Gibbs free energy of the optimal reaction pathway for CO_2RR on the Nb_1@qHP-C_{60} system at potentials of 0 V and −0.41 V.

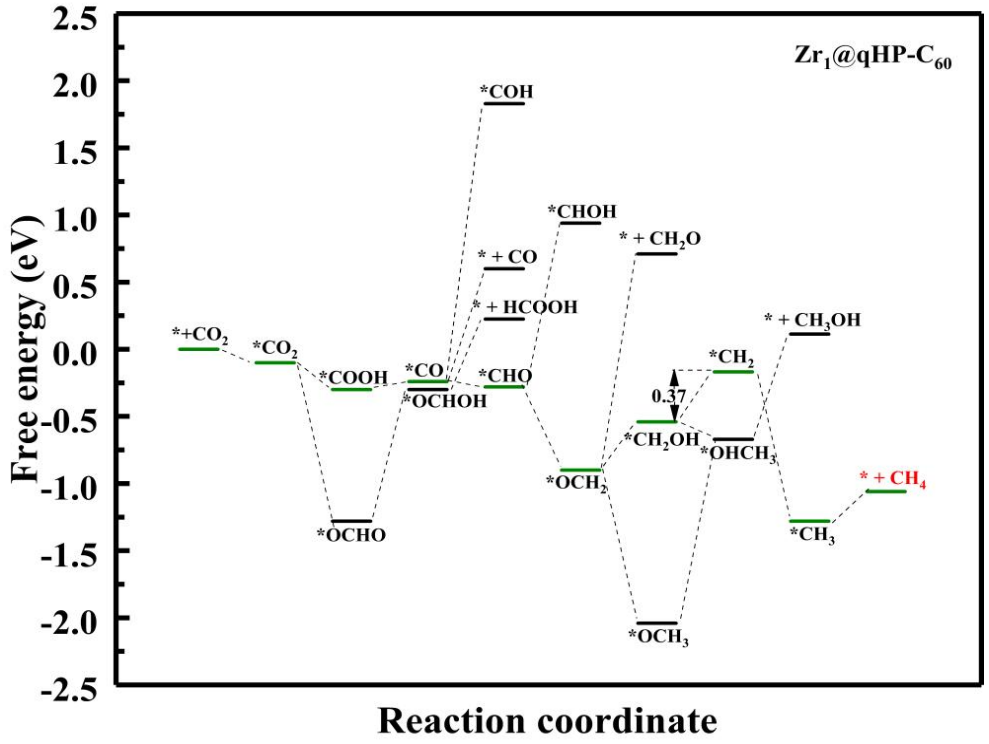

Fig. S10 The lowest energy pathways for CO_2RR to various products on the Zr_1@qHP-C_{60} system (in the absence of an applied potential).

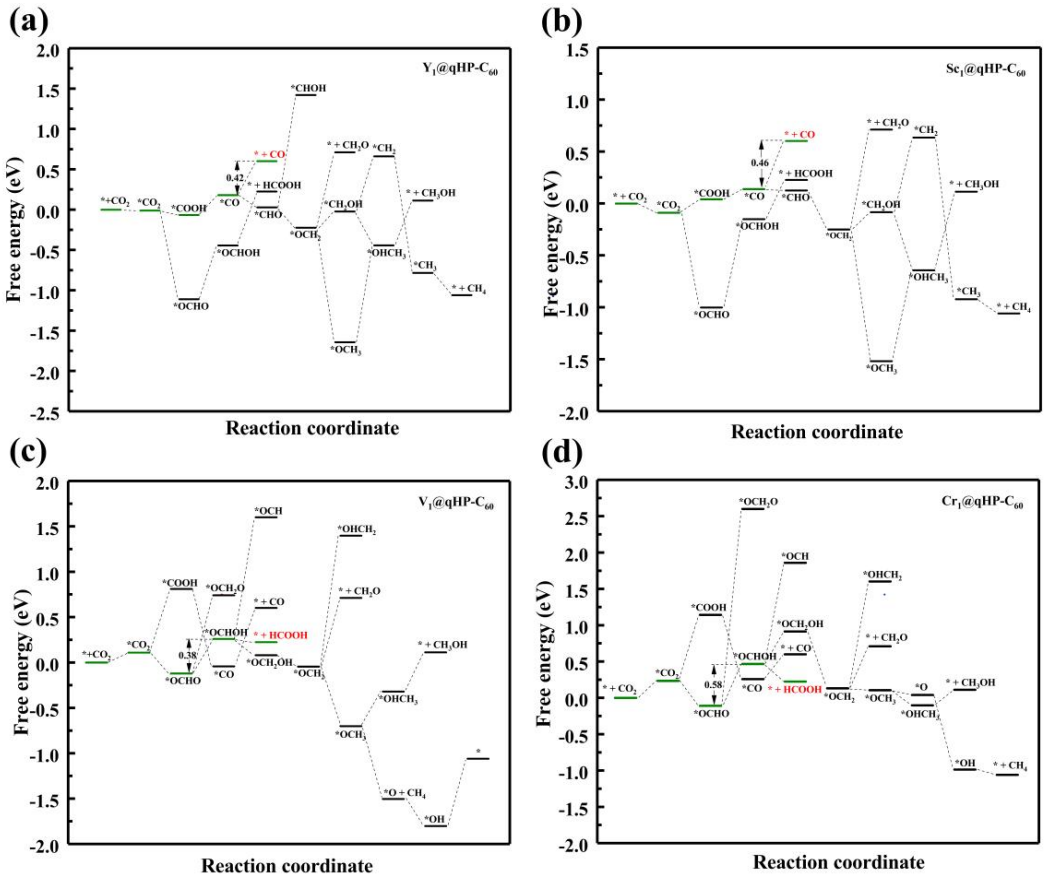

Fig. S11 The lowest energy pathways for CO_2RR to various products on the TM_1@qHP-C_{60} systems (TM = Y, Sc, V, Cr) in the absence of an applied potential are as follows: (a) Y_1@qHP-C_{60}; (b) Sc_1@qHP-C_{60}; (c) V_1@qHP-C_{60}; (d) Cr_1@qHP-C_{60}.

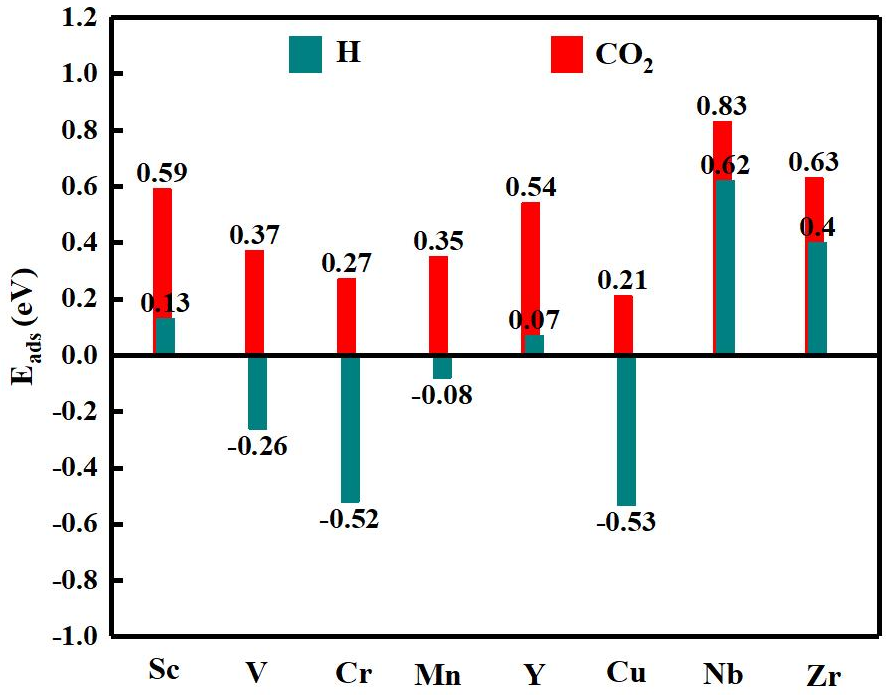

Fig. S12 Calculated adsorption energy (E_{ads}) for both H and CO_2 on TM_1@qHP-C_{60} (TM = Sc, V, Cr, Mn, Y, Cu, Nb, and Zr).

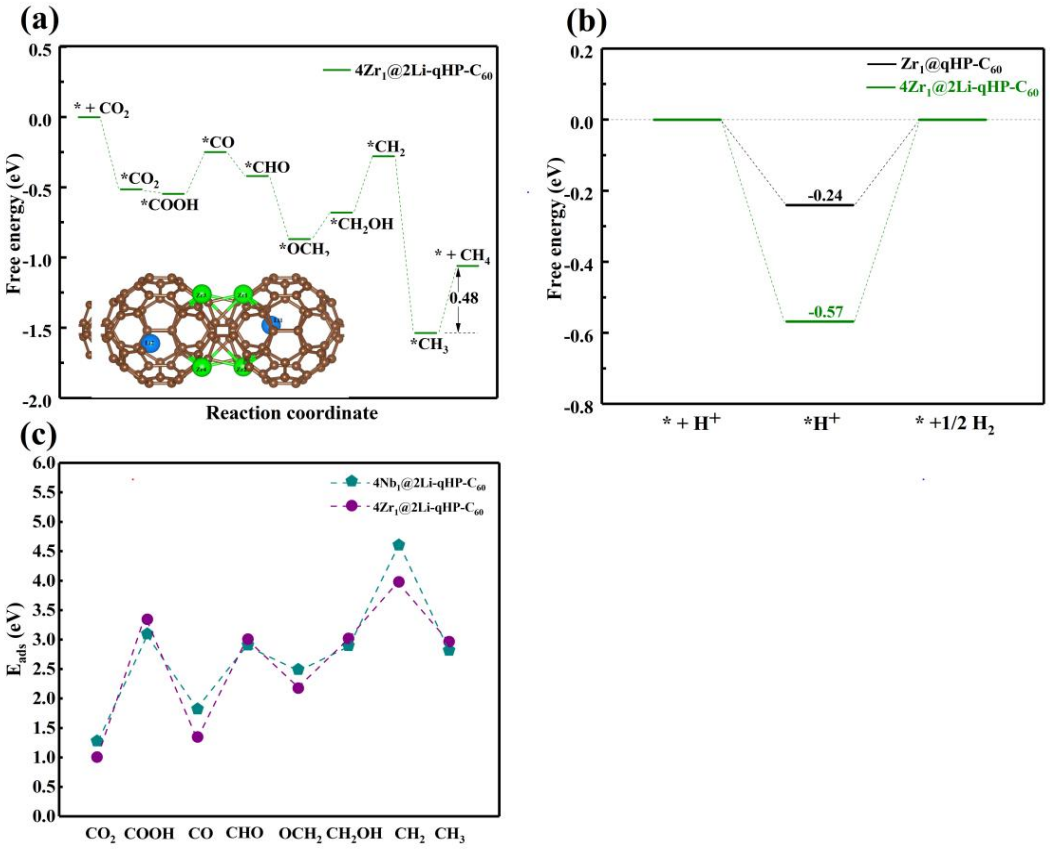

Fig. S13 (a) Gibbs free energy of the CH_4 formation pathway on the $4Zr_1$@2Li-qHP-C_{60} system; (b) Gibbs free energy of HER for Zr_1@qHP-C_{60} and $4Zr_1$@2Li-qHP-C_{60} systems; (c) Adsorption energies of intermediates in the CH_4 pathway on $4Nb_1$@2Li-qHP-C_{60} and $4Zr_1$@2Li-qHP-C_{60} systems.

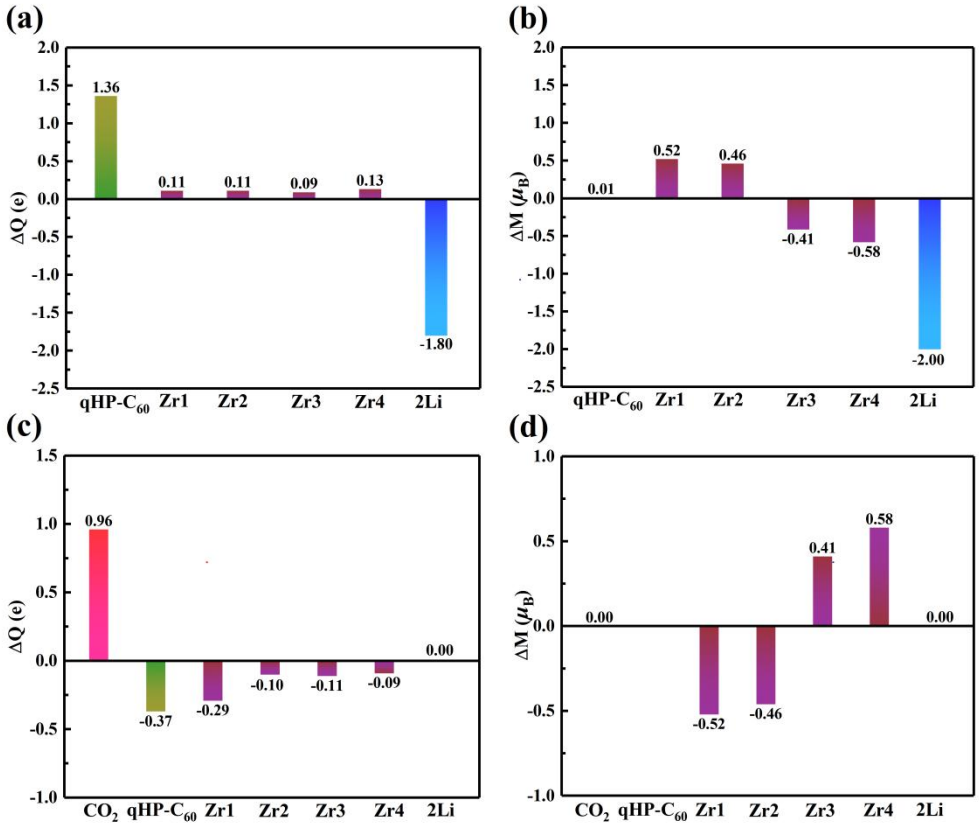

Fig. S14 Charge (a) and magnetic moment (b) variations of each component upon embedding two Li atoms into the $4Zr_1$@qHP-C_{60} system; Charge (c) and magnetic moment (d) variations of each component during CO_2 adsorption on the $4Zr_1$@2Li-qHP-C_{60} system.

Table S1 The structural parameters of CO_2 after adsorption on TM_1@qHP-C_{60} (TM = Nb, Zr, Cr) include the O-C-O bond angle, the C-O bond length, the TM-CO_2 distance, and the corresponding charge transfer.

	∠O-C-O (°)	O_1-C (Å)	O_2-C (Å)	(C)O_2-TM (Å)	Δ Q (e)
CO_2 (gas)	180.00	1.18	1.18	/	
Nb_1@qHP-C_{60}	135.08	1.22	1.33	(2.13) 2.10	0.76
Zr_1@qHP-C_{60}	179.43	1.17	1.19	2.40	-0.01
Cr_1@qHP-C_{60}	179.81	1.18	1.18	2.53	0.02

Table S2 Calculated spin moment variation contributed from qHP-C_{60} substrate ($\Delta M_{qHP\text{-}C60}$) and TM single atom ($\Delta M_{TM}$) and CO_2 species (ΔM_{CO2}) upon CO_2 adsorption. The adsorption energies (E_{ads}) are also provided.

TM_1/qHP-C_{60}	ΔM_{TM} (μ_B)	ΔM_{CO2} (μ_B)	$\Delta M_{qHP\text{-}C60}$ (μ_B)	$E_{ads}(CO_2)$(eV)
Nb	-0.52	0	+0.52	0.83
Zr	-0.08	-0.01	0.09	0.63
Sc	-0.06	0	-0.06	0.59
Y	-0.02	0	0.02	0.54
V	-0.05	0.06	-0.01	0.37
Cr	-0.05	0.05	0.00	0.27

Table S3 Comparison of CO_2RR performance between our optimal single-atom catalysts (SACs) and representative SACs reported in previous literature.

catalytic system	product	ΔG (eV)	source
Fe-TCSAC	CO	0.57	*J. Am. Chem. Soc.* **2025**, 147, 20318-20328
CuZn-SAs/NC	CH_4	0.76	*Chem. Eng. J.* **2023**, 471, 144618
Zr-MOF-In	HCOOH	0.49	*Angew. Chem. Int. Ed*. **2025**, 137, e202511132
Ag_1@NCNT Ag_1-AgAC@NCNT	CO	1	*Adv. Energy Mater.* **2024**, 14, 2400143
Ni_3-N-C	CO	0.45	*Angew. Chem. Int. Ed*. **2026**, 65, e18107